International Journal of Mechanical, Industrial and Aerospace Sciences
ISSN: 2517-9950
Vol:9, No:6, 2015

Gimbal Structure for the Design of 3D Flywheel System

Cheng-En Tsai, Chung-Chun Hsiao, Fu-Yuan Chang, Liang-Lun Lan, Jia-Ying Tu

***Abstract*—**New design of three dimensional (3D) flywheel system based on gimbal and gyro mechanics is proposed. The 3D flywheel device utilizes the rotational motion of three spherical shells and the conservation of angular momentum to achieve planar locomotion. Actuators mounted to the ring-shape frames are installed within the system to drive the spherical shells to rotate, for the purpose of steering and stabilization. Similar to the design of 2D flywheel system, it is expected that the spherical shells may function like a "flyball" to store and supply mechanical energy; additionally, in comparison with typical single-wheel and spherical robots, the 3D flywheel can be used for developing omnidirectional robotic systems with better mobility. The Lagrangian method is applied to derive the equation of motion of the 3D flywheel system, and simulation studies are presented to verify the proposed design.

***Keywords*—**Gimbal, spherical robot, gyroscope, Lagrangian formulation, flyball.

I. Introduction

MODERN vehicle and many robotic systems utilize multi-wheel and tire devices to contact with ground in order to maintain static equilibrium. The steering mechanism and suspension system control the motion and direction of wheels; in addition, the friction forces generated between wheels and ground exert the vehicle/robot to move. However, the complicated mechanism and a plurality of tires not only increase the weight of the vehicle/robot, but also cause more energy loss in the power transmission processes.

Considering the improvement on robotic system design, single-wheel robots which look like unicycles are proposed [1]. The actuator and associated power devices are embedded and enclosed within the robot with better protection against the environmental disturbances, thus giving more robust operation of the system, compared to other legged or wheeled robots. As the number of wheel decreases, the steering mechanism may be simplified to reduce the overall weight and energy loss. Furthermore, specialized mechanism for the purpose of stabilization and control need to be developed. For example, a single-wheel robot, *Gyrover*, is introduced in [2], [3]. Reference [2] uses flywheels and disks to balance the robot in the face of turning or tilting, and a gyroscope device is used in [3] to lean the robot body to left or right to change the direction of motion.

Though the design of single-wheel robots has the advantages of simplified mechanism and higher mobility, there are several issues need to be addressed as follows: (a) the balance control of the robot is relatively difficult, because the system has only one point in contact with ground; (b) the low-speed stability is difficult to maintain; (c) in the face of sudden impact, the robot may not be able to return to its stable attitude.

With the similar advantages to single-wheel robot, the ideal of spherical robot is proposed in the literature. According to the design of steering mechanism, the spherical robots can be divided into two types. The first type uses mechanical devices to adjust the center of gravity and generate eccentric moment to cause turning [4]-[6]; the second uses the principle of conservation of angular momentum to turn the robot [7], [8]. Take the design in [6] as an example of the first type, the robot uses the motion of four spokes to change the center of gravity. The four spokes lie in a tetrahedral structure, and each spoke contains a stepper-motor, a cylindrical screw, and a mass component. Therefore, as the motors apply torques to move the masses along the screws, the center of gravity of the robot changes. Another spherical robot in [8] is designed based on the second principle of conservation of angular momentum, where a motor is mounted to the center of gravity, and the rotor is connected to a mass. When the rotor spins, a reaction torque generated changes the direction of motion of the robot.

However, the above spherical robot designs present challenge in controlling the propulsion force and making the trajectory plan, because the dynamic model between the gravity-induced force/torque and the rolling velocity is difficult to determine [9]. Therefore, the gimbal-like spherical robotic designs are proposed, for example, the micro air vehicle in [10]. The gimbal-based robot installs motors to directly rotate the exterior structure, like a ring or a spherical shell; thus, the resulting trajectory and velocity are relatively straightforward to determine, in comparison with the pendulum-driven robots. In addition, the inner gimbal system enables the robot to turn, roll, and balance omnidirectonally, showing "intelligent" dynamics and motion.

The discussion about some of the existing vehicle and robotic systems motivates a novel 3D flywheel design in this paper. It equips with a gimbal-like mechanism to balance and control the motion of the system, and can be considered a robotic or vehicle system. Therefore, the next section of this paper will introduce the concepts of the 3D flywheel system. The Lagrangian method is used to derive the equations of motion of this system in Section III. Based on the results from

Research supported by the Taiwan Ministry of Science and Technology under grant MOST 102-2221-E-007-109-MY2.

C.-E. Tsai, C.-C. Hsiao, F.-Y. Chang, L.-L. Lan is with the Department of Power Mechanical Engineering, National Tsing Hua University, 300, Taiwan (R.O.C.) (e-mail: tsai_chenen@hotmail.com, en54612002@hotmail.com, acc0901@gmail.com, allan.lan456@gmail.com).

J.-Y. Tu is with the Department of Power Mechanical Engineering, National Tsing Hua University, 300, Taiwan(R.O.C.) (Tel.: +886-(0)3-57-42497; email: jytu@pme.nthu.edu.tw).

the previous sections, simulation studies were conducted in the MATLAB/Simulink environment to validate the proposed design. Finally, conclusion and future work will be provided.

TABLE I
NOTATIONS AND PARAMETERS FOR 3DF VEHICLE

Symbol	Description	Value
x_G	x-axis displacement of center of gravity	N/A
α_1	rotation angle of α-axis actuator	N/A
β_2	rotation angle of β-axis actuator	N/A
I_1	moment of inertia of outer shell	96.9 kg·m^2
I_2	moment of inertia of middle shell	72.9 kg·m^2
J_1	moment of inertia of outer frame	2.7 kg·m^2
M_1	mass of outer shell	146.8 kg
M_2	mass of middle shell	173.1 kg
m_1	mass of outer frame	5.0 kg
R_1	radius of outer shell	1.0 m
R_2	radius of middle shell	0.8 m
r_1	radius of outer frame	0.9 m
τ_α	output torque of α-axis actuator	N/A
τ_β	output torque of β-axis actuator	N/A
μ	coefficient of static friction	0.8

II. THE DESIGN OF 3D FLYWHEEL SYSTEM

In this section, the conceptual design of the proposed 3D flywheel system is presented. The front view and side view of the system are illustrated in Fig. 1 [11]; the main components contain three spherical shells, two frames, and a platform. The three shells are called outer shell, middle shell, and inner shell, respectively. The outer and middle shells are connected to the outer frame; the middle and inner shells are in connection with the inner frame. Three set of heteroaxial actuators which are perpendicular to each other are installed on the frames. Therefore, the rotation axes of the three shells are defined as α axis, β axis, and γ axis, respectively. Furthermore, the platform is connected to the inner shell, which can be used for mounting the power and control devices.

As shown in Fig. 1, the outer, middle, and inner shells are actuated by the α-axis, β-axis, and γ-axis actuators, respectively. The α-axis and β-axis actuators are mounted to the outer frame, and the γ-axis actuator is fixed to the inner frame. The α-axis actuator drives the outer shell to rotate forward/backward and achieve rectilinear motion. Rotations of the middle and inner shells exerted by the β-axis and γ-axis actuators are responsible for turning and balancing the system. Furthermore, within the inner shell the platform may equip with electronic and control devices, such as batteries, motors, and sensors, for the control, operation, and monitoring purposes. Additional mechanism, such as pendulums or 2D flywheels, can be considered and mounted to the platform, for advanced stabilization and attitude control.

Future control system and signal processing design is shown in Fig. 2, where the destination and route planning may be computed by a remote control center, which transmits the path commands to the control system of the 3D flywheel. Then, the 3D flywheel controller computes the control signals to drive the actuators to rotate the shells. Sensors measure the in-motion signals, such as torques, velocity, and rotation angle, and send the signals back to the controller. According to the measured signals, the controller compares the reference and output signals to modify the control signals. Meanwhile, the controller sends the current position to the remote control center for path tracking.

Unlike many other robotic and vehicle systems which depend on multiple wheels to make a contact plane to maintain static equilibrium and achieve rectilinear motion, the exterior structure of the 3D flywheel only has a single contact point with ground. Therefore, it is possible that the 3D flywheel can be used as an omnidirectional robot with higher mobility. In addition, with precise dynamic modeling and intelligent control, the spherical shells are able to store and supply energy like a 2D flywheel; this will be further introduced in the simulation study of Section IV.

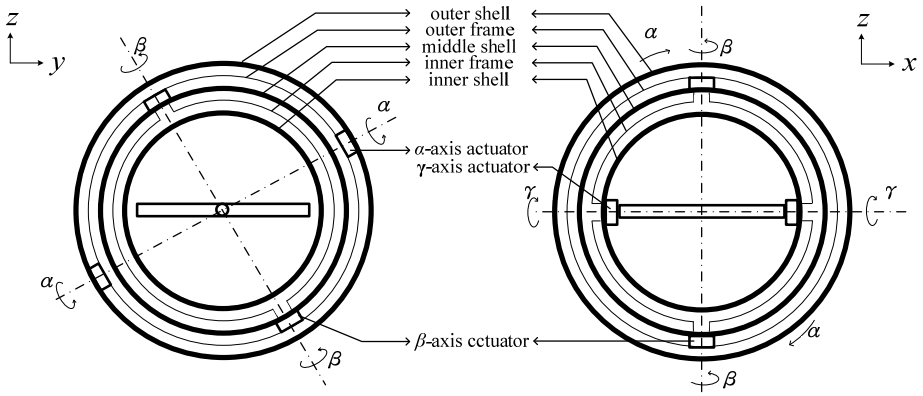

(a) Front view (b) Side view

Fig. 1 The scheme of 3D flywheel system [11]

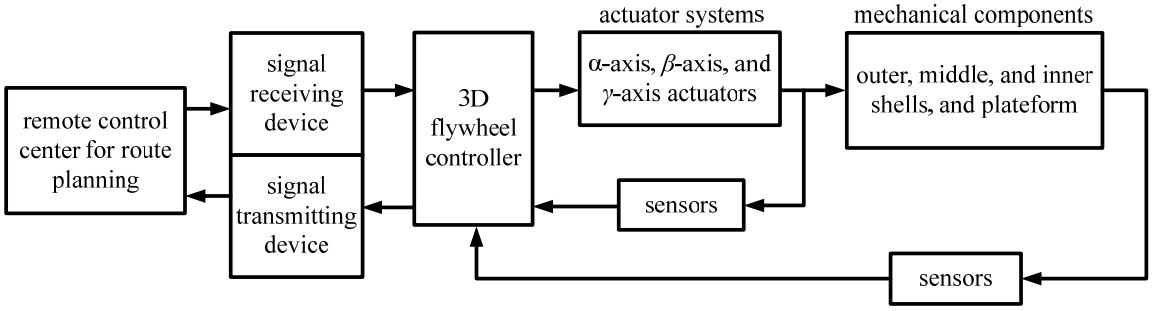

Fig. 2 The scheme of 3D flywheel control system with remote control

III. Derivation of System Dynamics

This section uses the Lagrangian formulation to derive the dynamic model of the 3D flywheel system. First of all, the operation conditions are introduced, which can be divided into two parts. One is the rectilinear motion, and the other is the turning motion. In the rectilinear motion along the *x*-axis direction, as shown in Fig. 3, the *α*-axis actuator rolls the outer shell to move forward/backward. In this case, the *β*-axis and *γ*-axis actuators may slightly rotate the middle and inner shells to balance and stabilize the platform and the entire system.

Furthermore, in the turning case, the rotation of the middle shell related to the *β*-axis actuator needs to be considered. The *α*-axis actuator and outer shell dominate the forward and backward locomotion, and the *β*-axis actuator and middle shell are used to turn the 3D flywheel system toward left or right. When the middle shell rotates, it generates a reaction moment to rotate the outer shell in a different orientation. Meanwhile, the rotation of the inner shell related to the *γ*-axis actuator balances the platform and produces a reaction moment to the entire system to make the turning motion smooth, as shown in Fig. 4.

In the following subsections, only the outer shell, middle shell, outer frame, *α*-axis actuator, and *β*-axis actuator are considered, for the sake of brevity. The *x*-axis equation of motion of the 3D flywheel is discussed first, followed by the spinning dynamics.

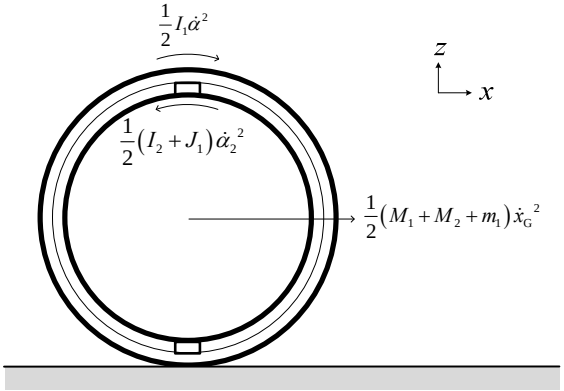

Fig. 3 The scheme of *x*-axis kinetic energy

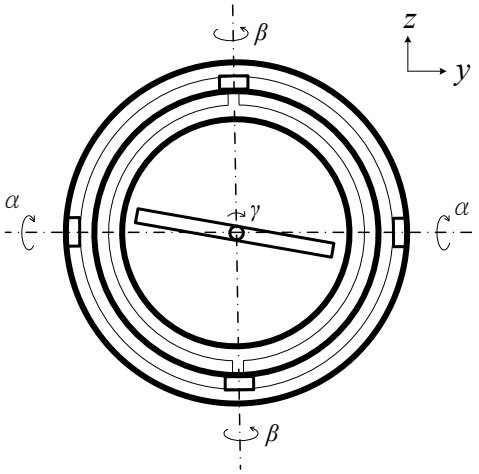

(a) Turn right

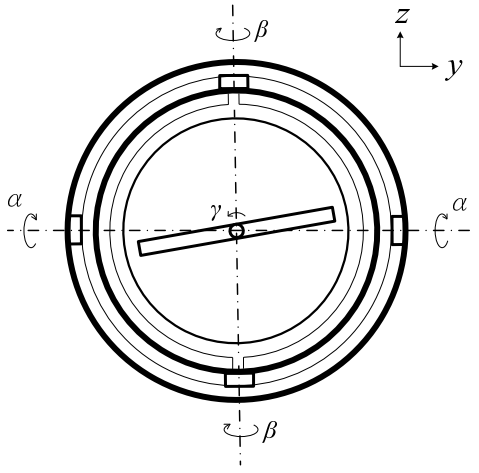

(b) Turn left

Fig. 4 The operation scheme of 3D flywheel when turning

A. The x-Axis Equation of Motion

Here, the Lagrangian method is used for deriving the *x*-axis equation of motion. The general form of Lagrange equation is written as

$$\frac{d}{dt}\left(\frac{\partial L}{\partial \dot{q}_i}\right)-\frac{\partial L}{\partial q_i}=Q_i,\ i=1,2,...,n \tag{1}$$

where L is called Lagrangian, defined as the difference between the kinetic energy, T, and the potential energy, V, written as $L = T - V$. The generalized force and coordinate are represented by Q_i and q_i, respectively, and n denotes the number of degree of freedom.

According to (1) and Fig. 3, the α-axis dynamics related to the rotation angle and angular velocity is defined as the generalized coordinate, and the torque generated from the α-axis actuator, τ_α, is defined as the generalized force. The scheme of *x*-axis kinetic energy is shown in Fig. 3, and the dynamic model considers the system is rolling without slipping. Therefore, the velocity of the center of gravity, $\dot{x}_G$, is written as

$$\dot{x}_G = R_1\dot{\alpha}_1 \tag{2}$$

where R_1 is the radius of the outer shell, and α_1 is the rotation angle of the outer shell with respect to ground. As the α-axis actuator produces torque to rotate the outer shell, a reaction torque also applies to the outer frame. As a result, the outer frame and middle shell together rotate in an opposite direction; the total kinetic energy is represented by

$$T=\frac{1}{2}\left[I_1+\left(M_1+M_2+m_1\right)R_1^{\,2}\right]\dot{\alpha}_1^2 \tag{3}$$

where I_1 is the moment of inertia of the outer shell, and M_1, M_2, and m_1 are the masses of the outer shell, middle shell, and outer frame, respectively. In addition, the potential energy of this system yields

$$V=\left(M_1+M_2+m_1\right)gR_1. \tag{4}$$

Therefore, subtracting (4) from (3) gives the Lagrangian L. With the substitution of L into (1), the Lagrange equation is expanded and becomes

$$\left[I_1+\left(M_1+M_2+m_1\right)R_1^{\,2}\right]\ddot{\alpha}=\tau_\alpha \tag{5}$$

which shows the *x*-axis equation of motion.

B. The β-Axis Spinning Dynamics

This section further discusses the spinning dynamics of the 3D flywheel, as shown in Fig. 5. In this case, the β-axis actuator rotates the middle shell and generates a reaction torque to spin the outer shell along the β axis, and the α-axis actuator does not apply any torque. Here, the rotation angle of middle shell generated by the β-axis actuator is denoted as β_2; in addition, the rotation angle due to the reaction torque that spins the outer frame and outer shell is denoted as β_1. Thus, the kinetic energy related to the β-axis dynamics are given by

$$T=\frac{1}{2}\left(I_1+J_1\right)\dot{\beta}_1^2+\frac{1}{2}I_2\left(\dot{\beta}_1-\dot{\beta}_2\right)^2, \tag{6}$$

where J_1 and I_2 denote the moments of inertia of the outer frame and middle shell, respectively. In addition, the potential energy of the 3D flywheel has been given in (4). Therefore, the Lagrangian is obtained by subtracting (4) from (6) as follows

$$L=\frac{1}{2}\left(I_1+J_1\right)\dot{\beta}_1^2+\frac{1}{2}I_2\left(\dot{\beta}_1-\dot{\beta}_2\right)^2-\left(M_1+M_2+m_1\right)gR_1. \tag{7}$$

Assuming that the friction torque acting on the outer shell is denoted as τ_f, the generalized coordinate and force are defined as $q_1 = \beta_1$ and $Q_1 = \tau_f$, respectively. As a result, substituting τ_f and (7) into (1) gives the following Lagrange equation and the equation of motion

$$\frac{d}{dt}\left(\frac{\partial L}{\partial \dot{\beta}_1}\right)-\frac{\partial L}{\partial \beta_1}=\tau_f, \tag{8}$$

$$\ddot{\beta}_1=\frac{1}{\left(I_1+J_1+I_2\right)}\tau_f+\frac{I_2}{\left(I_1+J_1+I_2\right)}\ddot{\beta}_2. \tag{9}$$

Furthermore, considering the moment of momentum theorem, the applied torque related to $\ddot{\beta}_2$ yields

$$\tau_f+\tau_\beta=(I_1+J_1+I_2)\ddot{\beta}_2. \tag{10}$$

Thus, (6)-(10) shows the β-axis spinning dynamics. However, the coupled dynamics between each axis and the rotation of the inner shell are not included in the discussion, which will be considered in the authors' future work.

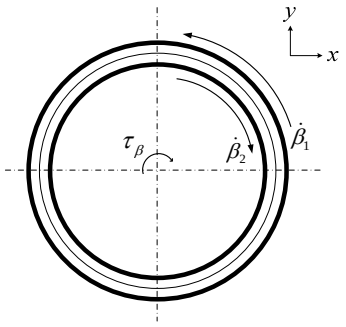

Fig. 5 The scheme of the β-axis spinning motion [11]

IV. Simulation Studies and Implementation Work

In this section, the scheme of Fig. 3 is built in the graphical user interface for simulation validation. The model contains outer shell, middle shell, outer frame, α-axis actuators, and β-axis actuators, corresponding to the scheme of Fig. 3. For brevity, the simulation work considers only the *x*-axis motion, leading to the discussion about the 3D flywheel design for

storing and supplying mechanical energy. (The preliminary simulation results of planar motion on the *x*-*y* plane can be referred to in [11].) Figs. 6 and 7 present the simulation results, with the simulation time set to 25 seconds.

As shown in Fig. 6, the α-axis actuator applied negative torque to rotate the outer shell, and the 3D flywheel rolled forward. Fig. 6 (a) displays the torque signal of the α-axis actuator, where the torque was given in the first three seconds with a maximum magnitude of 3000 Nm. The torque accelerated the 3D flywheel, and the angular velocity of the outer shell increased to a peak of -900 deg/s, as shown in Fig. 6 (b). When the torque was reduced to zero, the system gradually decelerated due to the friction force between the outer shell and ground. Accordingly, the resulting *x*-axis displacement and velocity, x_G and $\dot{x}_G$, are depicted in Figs. 6 (c) and Fig. 6(d), respectively. Importantly, although the torque signal was null in the 3rd to 25th seconds, Figs. 6 (b)-(d) show that the stored energy in the acceleration process rolled the 3D flywheel system continuously. This verifies the concept of using the 3D flywheel design for storing and supplying mechanical energy. The results are verified again in Figs. 7 (a)-(d), with the applied torque in a different direction, and hence the 3D flywheel rolled backward.

In addition to the preliminary simulation results, a prototype of the 3D flywheel is shown in Fig. 8, which is temporally called a 3D flywheel robot. The major components in the robot include a plastic outer shell, an outer frame, and a platform; the control and power units are mounted to the platform. Two motors are taken as the set of the α-axis actuator to roll the robot. Additional motors and spinning disks are installed to balance and steer the system. Testing of the robot comprises the authors' ongoing work.

V. Conclusion

In this paper, a novel design of 3D flywheel system is proposed. The design includes three spherical shells and two frames, and they are connected like a gimbal structure. The shells are equipped with motors to generate torque and roll the system, achieving the planar locomotion. With precise control to the rotation of the spherical shells, it is expected that the 3D flywheel system would possess intelligent and fast responses like the gyroscope dynamics, and the author would name the system as "flyball". The *x*-axis equation of motion and spinning dynamics are derived by the Lagrangian formulation, and the simulation results verify the *x*-axis motion. In future work, the complete coupled dynamics and equations of motion of the system will be derived. In addition, advanced control system design for stabilization and rapid steering will be considered.

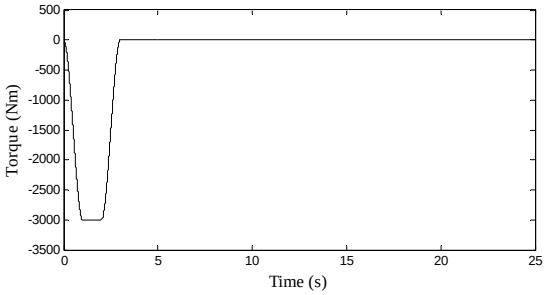

(a) The driving torque of the α-axis actuator

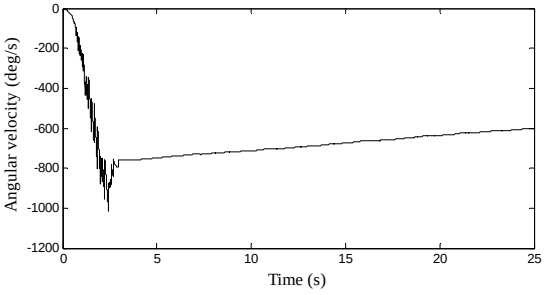

(b) Angular velocity of the outer shell

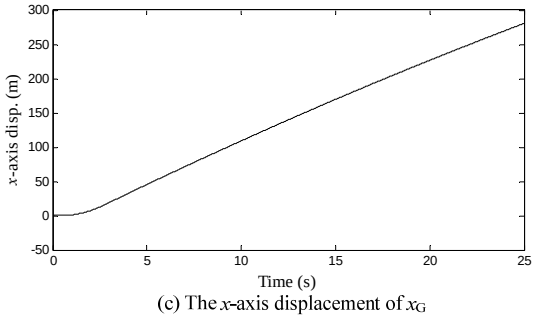

(c) The *x*-axis displacement of x_G

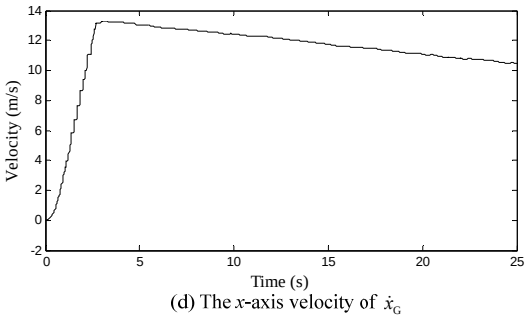

(d) The *x*-axis velocity of $\dot{x}_G$

Fig. 6 Simulation results of forward locomotion

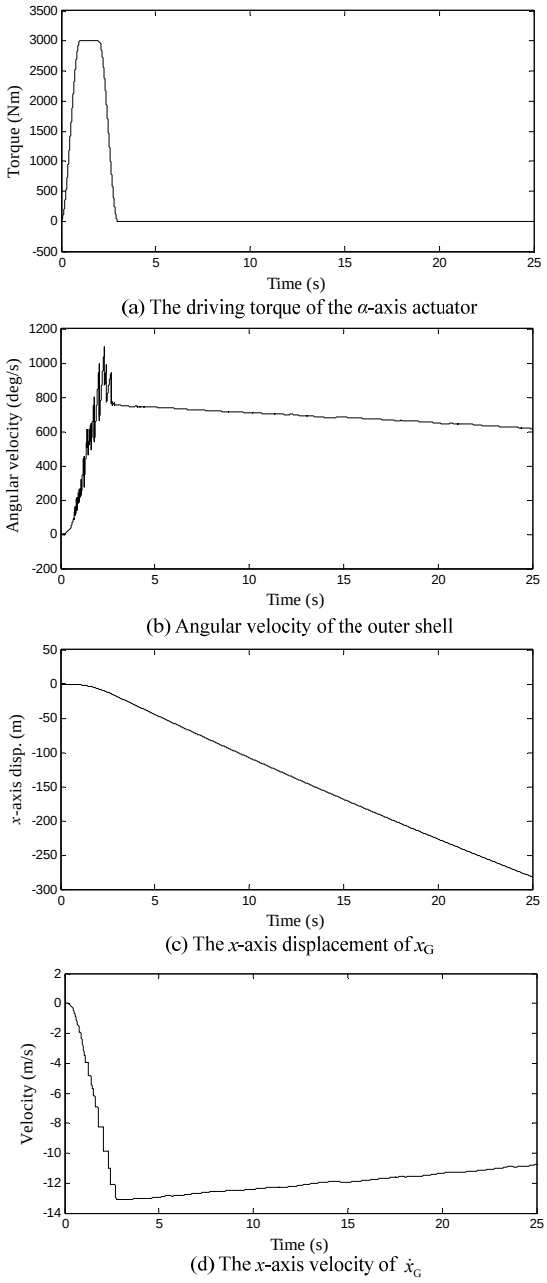

Fig. 7 Simulation results of backward locomotion

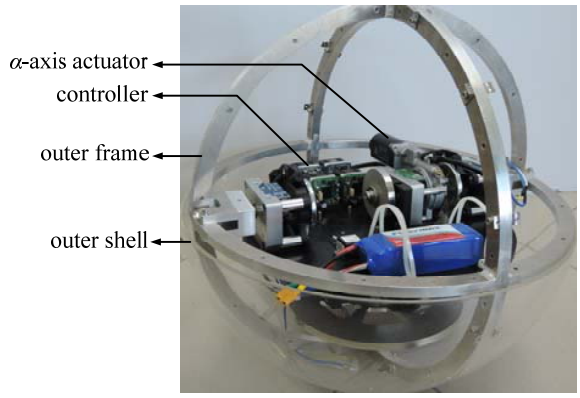

Fig. 8 The prototype of the 3D flywheel robot [11]

ACKNOWLEDGMENT

The authors gratefully acknowledge the support of Taiwan Ministry of Science and Technology, under grant MOST 102-2221-E-007-109- MY2 "*Evaluation of Optimal Dynamic Substructuring Tests: Development and Application of Substructurability Theory*', for their support in the pursuance of this work. Also, the authors are grateful to the National Center for High-performance Computing for computer time and facilities.

REFERENCES

[1] H. B. Brown, Jr. and X. Yangsheng, "A single-wheel, gyroscopically stabilized robot," *IEEE International Conference on Robotics and Automation*, New York, NY, USA, 1996, pp. 3658-3663.

[2] G. C. Nandy and X. Yangsheng, "Dynamic model of a gyroscopic wheel," *IEEE International Conference on Robotics and Automation*, New York, NY, USA, 1998, pp. 2683-2688.

[3] S. J. Tsai, E. D. Ferreira, and C. J. J. Paredis, "Control of the gyrover," *IEEE/RSJ International Conference on Intelligent Robots and Systems: Human and Environment Friendly Robots whith High Intelligence and Emotional Quotients*, Kyongju, South Korea, 1999, pp. 179-184.

[4] A. Halme, T. Schonberg, and W. Yan, "Motion control of a spherical mobile robot," *IEEE International Workshop on Advanced Motion Control*, New York, NY, USA, 1996, pp. 259-264.

[5] A. Bicchi, A. Balluchi, D. Prattichizzo, and A. Gorelli, "Introducing the `SPHERICLE': An experimental testbed for research and teaching in nonholonomy," *IEEE International Conference on Robotics and Automation*, Albuquerque, NM, USA, 1997, pp. 2620-2625.

[6] A. A. H. Javadi and P. Mojabi, "Introducing August: a novel strategy for an omnidirectional spherical rolling robot," Piscataway, NJ, USA, 2002, pp. 3527-3533.

[7] S. Bhattacharya and S. K. Agrawal, "Spherical rolling robot: A design and motion planning studies," *IEEE Transactions on Robotics and Automation,* vol. 16, pp. 835-839, 2000.

[8] G. Shu, Q. Zhan, and Y. Cai, "Motion control of spherical robot based on conservation of angular momentum," *IEEE International Conference on Mechatronics and Automation*, Changchun, China, 2009, pp. 599-604.

[9] W.-H. Chen, C.-P. Chen, W.-S. Yu, C.-H. Lin, and P.-C. Lin, "Design and implementation of an omnidirectional spherical robot Omnicron," *IEEE/ASME International Conference on Advanced Intelligent Mechatronics (AIM)*, Piscataway, NJ, USA, 2012, pp. 719-24.

[10] C. E. Thorne and M. Yim, "Design and analysis of a gyroscopically controlled micro air vehicle," *Journal of Intelligent & Robotic Systems,* vol. 65, pp. 417-35, 2012.

[11] C.-C. Hsiao, C.-E. Tsai, J.-Y. Tu, and Y.-K. Ting, "Development of a Three-Dimensional-Flywheel Robotic System," *International Conference on Mechanical Engineering and Applied Mechanics*, Paris, France, 2015.